Published by IOP Publishing for Sissa Medialab

Received: *October 17, 2022*
Revised: *December 30, 2022*
Accepted: *January 18, 2023*
Published: *February 2, 2023*

Check on the features of potted 20-inch PMTs with 1F3 electronics prototype at Pan-Asia

Caimei Liu,[a,b] **Min Li,**[a,b] **Zhimin Wang,**[a,b,*] **Jun Hu,**[a] **Nikolay Anfimov,**[f] **Lei Fan,**[a] **Alberto Garfagnini,**[g] **Guanghua Gong,**[h] **Shaojing Hou,**[a] **Xiaolu Ji,**[a] **Xiaoshan Jiang,**[a] **Denis Korablev,**[f] **Tobias Lachenmaier,**[c] **Si Ma,**[a] **Xiaoyan Ma,**[a] **Zhe Ning,**[a] **Alexander G. Olshevskiy,**[f] **Zhaoyuan Peng,**[a,b] **Zhonghua Qin,**[a] **Tobias Sterr,**[c] **Yunhua Sun,**[a] **Alexander Felix Tietzsch,**[c] **Jun Wang,**[e] **Wei Wang,**[e] **Yangfu Wang,**[a,b] **Kaile Wen,**[a] **Bjoern Soenke Wonsak,**[d] **Wan Xie,**[a] **Meihang Xu,**[a] **Xiongbo Yan,**[a,b] **Yifan Yang,**[i] **Rong Zhao,**[e] **Tong Zhou**[a,b] **and Kejun Zhu**[a]

[a] *Institute of High Energy Physics, Chinese Academy of Sciences, Beijing 100049, China*
[b] *University of Chinese Academy of Sciences, Beijing 100049, China*
[c] *Eberhard Karls Universität Tübingen, Physikalisches Institut, Tübingen, Germany*
[d] *Institute of Experimental Physics, University of Hamburg, Hamburg, Germany*
[e] *Sun Yat-Sen University, Guangzhou, China*
[f] *Joint Institute for Nuclear Research, Dubna, Russia*
[g] *Dipartimento di Fisica e Astronomia, Università di Padova and INFN Sezione di Padova, Padova, Italy*
[h] *Tsinghua University, Beijing, China*
[i] *Université Libre de Bruxelles, Brussels, Belgium*

E-mail: wangzhm@ihep.ac.cn

Abstract: The Jiangmen underground neutrino observatory (JUNO) is a neutrino project with a 20-kton liquid scintillator detector located 700-m underground. The large 20-inch PMTs are one of the crucial components of the JUNO experiment aiming for precision neutrino measurements with better than 3% energy resolution at 1 MeV. The excellent energy resolution and a large fiducial volume provide many exciting opportunities for addressing important topics in neutrino and astroparticle physics. With the container #D at JUNO Pan-Asia PMT testing and potting station, the features of waterproof potted 20-inch PMTs were measured with JUNO 1F3 electronics prototype in waveform and charge, which are valuable for a better understanding of the performance of the waterproof potted PMTs and the JUNO 1F3 electronics. In this paper, the basic features of the JUNO 1F3 electronics prototype run at Pan-Asia will be introduced, followed by an analysis of the waterproof potted 20-inch PMTs and a comparison with the results from commercial electronics used by container #A and #B.

Keywords: Data processing methods; Photon detectors for UV, visible and IR photons (vacuum) (photomultipliers, HPDs, others)

ArXiv ePrint: 2208.08264

*Corresponding author.

© 2023 IOP Publishing Ltd and Sissa Medialab
https://doi.org/10.1088/1748-0221/18/02/P02003

Contents

1 Introduction **1**

2 Container #D with 1F3 electronics prototype **2**

3 Results with container #D **5**
- 3.1 Noise level 5
- 3.2 Waveform parameters 5
- 3.3 Charge parameters 9

4 Comparison with commercial electronics **9**

5 Summary **12**

2023 JINST 18 P02003

1 Introduction

The measurement of θ_{13} by Daya Bay [1], RENO [2] and Double Chooz [3] provides a possibility to determine the neutrino mass ordering (NMO) with reactor neutrinos. The Jiangmen Underground Neutrino Observatory (JUNO) [4, 5], with a 20-kton multi-purpose underground liquid scintillator (LS) detector, as shown in figure 1, plans to use 20,000 20-inch PMTs [6] (15,000 Micro Channel Plate (MCP) PMTs from Northern Night Vision Technology Ltd. (NNVT GDB6201) [7] and 5,000 dynode PMTs from Hamamatsu Photonics K.K. (HPK R12860) [8]) for an excellent energy resolution of at least 3% at 1 MeV with higher than 75% PMT coverage. The PMTs' performance has a critical impact on the measurements of the energy, timing, and vertex of JUNO to ensure the NMO sensitivity.

Compared to the traditional HPK dynode PMTs, the selected 20-inch NNVT MCP-PMTs were specially developed for the JUNO experiment with a high quantum efficiency (QE) [10], where the MCP, a plate-like structure consisting of many thin glass tubes with semiconductor material coated [11], plays a key role in electron multiplication. There are two versions of MCP-PMTs identified by their production date: the low-QE PMTs from early production and the high-QE PMTs from late production with different production processes. The quantum efficiency of low-QE PMTs and high-QE PMTs has not been measured systematically. But overall, their average detection efficiency is about 27.3% and 31.3% respectively [12].

Both types of JUNO selected 20-inch PMTs are required to pass a visual inspection, an acceptance test (with a pluggable HV divider [13, 14]), and are finally potted to be waterproof (HV divider firmly soldered to the PMT) [15]. All of the 20-inch PMTs used for JUNO have been received and tested [12] in a container system [16] and a scanning system [17]. Each PMT was tested at least once during the process. A sub-sample of the potted PMTs was tested to check their features and consistency with the results of bare PMTs.

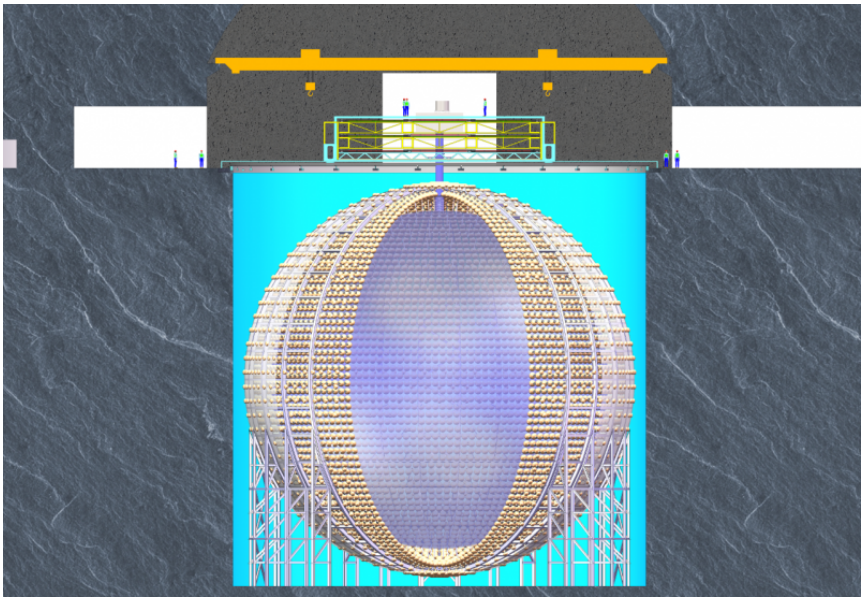


Figure 1. Schematic view of the JUNO detector [9].

The container system includes four containers. Containers #A and #B are configured for the mass acceptance test with commercial electronics, by which all the qualified 20,000 20-inch PMTs of JUNO were tested at least once. Container #C is used for long-term stability monitoring of some sampled PMTs with a set of commercial electronics. In the commercial electronics, CAEN A7030TP board in CAEN SY5527 power supply system can provide HV. CAEN V1742 switched-capacitor digitizer is used to waveform acquisition with a 12-bit resolution at 1 Vpp dynamic range and a sampling rate of up to 5 GS/s [18]. CAEN V895B leading edge discriminator board and CAEN V830AC 32-bit 32 channels latching scaler module are used for counting measurements. Container #D is equipped with JUNO 1F3 electronics prototype [15] to have combined testing with the potted 20-inch PMTs and JUNO 1F3 electronics. The 1F3 electronics is custom designed for a wide dynamic range from 1 p.e. to 1000 p.e. and a good linearity response [19]. In total, 6681 1F3 electronics UWBox (Under Water box) will be used for all 20-inch PMTs in JUNO. The testing with container #D provides an early understanding of the characteristics of JUNO 1F3 electronics with potted 20-inch PMTs.

In this paper, we will present the basic features of the JUNO 1F3 electronics, and the combined characteristics of the potted 20-inch PMTs with the 1F3 electronics. A brief introduction of container #D will be presented in section 2. The analysis and results will be shown in section 3. A comparison between the results with the 1F3 electronics prototype and commercial electronics is discussed in section 4. Finally, a summary is given in section 5.

2 Container #D with 1F3 electronics prototype

The primary facility used for the qualification of the 20-inch PMTs is the container system, which has been introduced in detail in a previous paper, including the mechanical setup, data-taking electronics, and the measurement process [16]. Only a brief description will be provided here for a better understanding of the following results, in particular for container #D. The containers

2023 JINST 18 P02003

work as darkrooms. Each container is shielded by six alternating layers of silicon-iron to reduce the influence of the geomagnetic field, leaving the residual magnetic field only 4.7 μT which is required by the future JUNO detector too. Container #D contains 32 testing channels (drawers), as shown in figure 2, in which a total of 11 GCUs (Global Control Unit) are installed (1 GCU for 3 electronics channels (1F3), 33 electronics channels in total). Each of the drawers is equipped with a stabilized LED light source [20], which illuminates the full photocathode uniformly with the help of a collimator, attenuator, diffuser, and cylindrical reflector, and each drawer box works independently. The wavelength of the light source is 420 nm, and its intensity can be configured for different purposes [21]. An HVAC (heating, ventilation, and air conditioning) unit is used to control the measurement environment inside the containers, which is configured to 23°C for container #D.

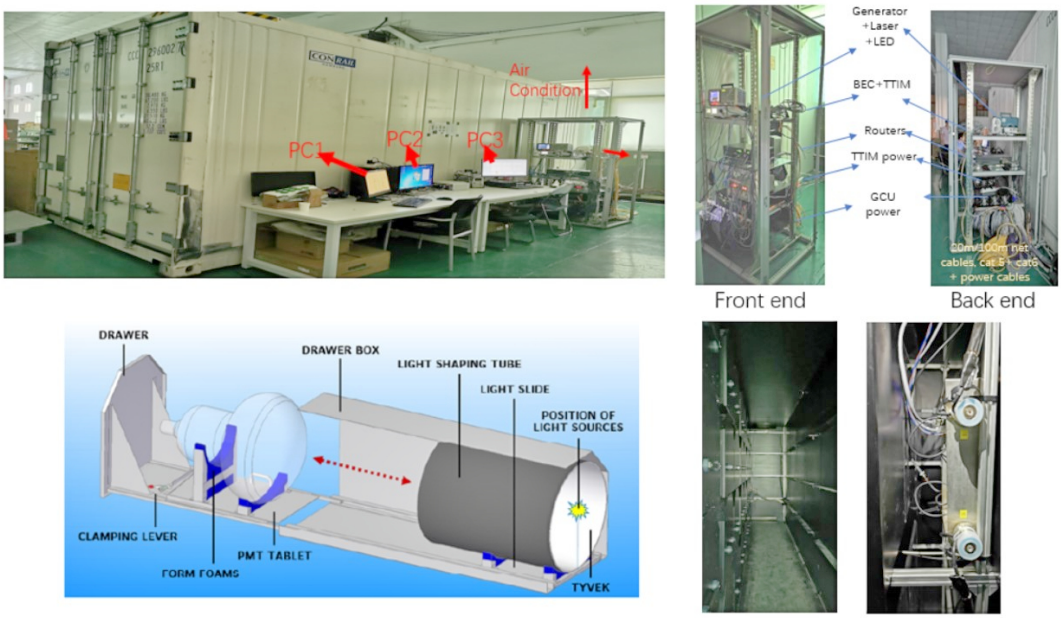


Figure 2. Top left: the outer view with control PCs of the 20-foot container of container #D. Top right: the rack where the power and net controller are installed. Bottom left: the schematic view of a drawer box. Bottom right: the internal view of the container and an installed box of JUNO 1F3 electronics between the drawers.

The JUNO 1F3 electronics prototype used by container #D is integrated with a high voltage unit (HVU) and a GCU,[1] as shown in figure 2. The custom HVU provides the bias voltage to PMTs. As the core of the readout electronics, the GCU is used for analog-digital conversion and waveform acquisition. After receiving the PMT signal, the GCU duplicates it into two streams with different amplification factors in the front-end chip and converts the current signal into voltage. Then the analog signal is converted into a digital signal by a 14 bits, 1 GS/s, custom ADC. The conversion factor from ADC to the amplitude of high gain is around 0.12 mV/ADC (dynamic range 1.2 V with 14-bit and an amplification of 0.6, keep two significant digits), which is used for the following analysis. Finally, the digital signal is further processed in the field-programmable gate array (FPGA), for local trigger generation, charge reconstruction, timestamp tagging, and temporary storage.

[1] An embedded version of the system can be found in [22].

2023 JINST 18 P02003

A DAQ system based on Linux is realized for container #D with the 1F3 electronics [23], which can provide the initialization, configurations of HVU and electronics, control and waveform readout, dark count rate (DCR) and temperature monitoring of each electronics channel. The DCR is the pulses per second with a configurable threshold relative to the baseline. The temperature monitoring of each electronics channel indicates the chip temperature will reach its stable status in around 20 minutes and can run smoothly in the configured air environment, as shown in figure 3. In addition, there is an almost 20°C temperature difference between GCUs close to the ventilation fan and GCUs further away. As a result, it seems that it does not affect the response parameters of PMTs. Of course, the temperature of the operating environment is expected to be uniform and stable, but the fact proves that the 1F3 electronics can still operate normally under the 20°C temperature difference.

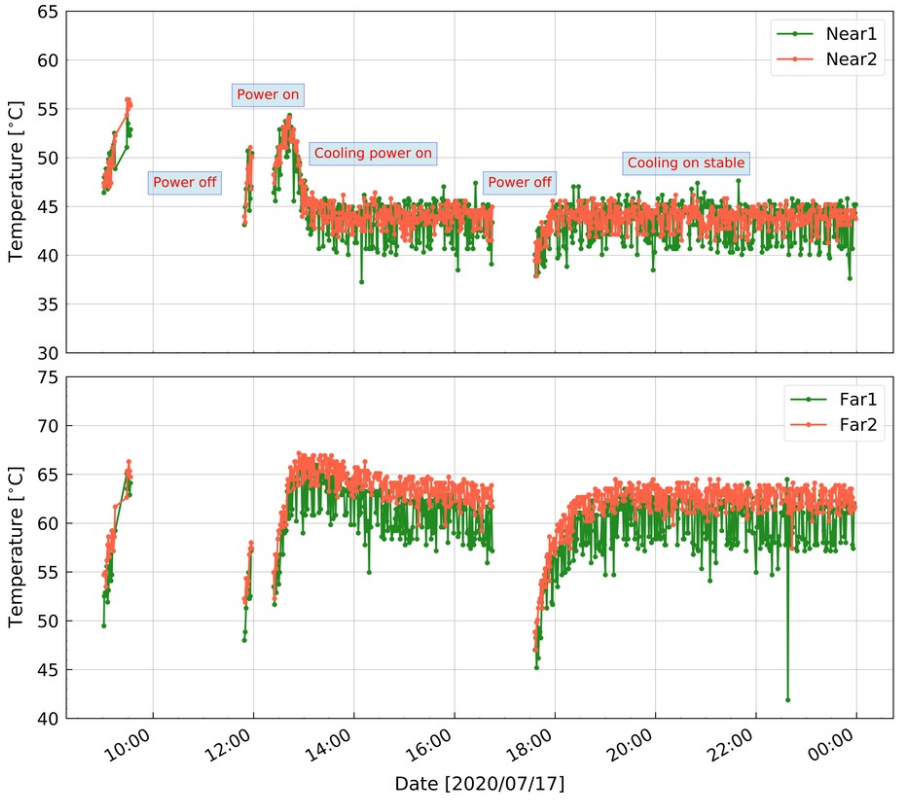


Figure 3. Temperature monitoring of the GCU channels (chips). Top: the temperature from two electronics channels from a single GCU near the container ventilation fan; bottom: the temperature from two electronics channels from another single GCU far from the container ventilation fan.

582 waterproof potted PMTs were tested in container #D as well as in containers #A or #B following the same procedure as in [16]. A cable of 2 m (for JUNO central detector) or 3 m (for JUNO veto detector) with a special SHV connector is soldered to the waterproof potted 20-inch PMT, where a stainless steel bellow is also used for pure water sealing. To make operation convenient in container #D, another 2 m extension cable is used between the potted PMT and the 1F3 box, which however affects the measured waveform shape.

2023 JINST 18 P02003

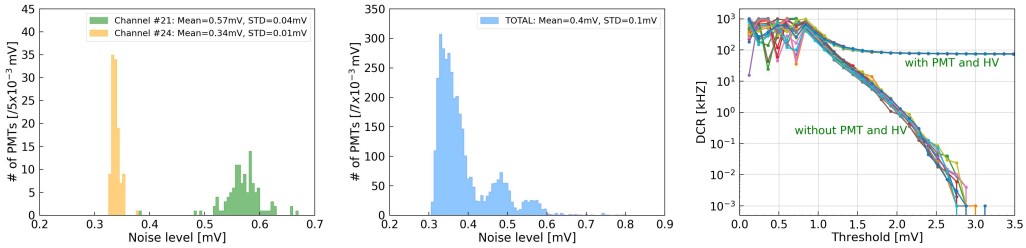
3 Results with container #D

Various parameters of potted PMTs such as timing, amplitude, and charge can be derived with the recorded waveforms. According to the testing procedure, all the parameters are checked for each PMT with container #D, including DCR, gain, peak-to-valley-ratio (P/V), signal-to-noise (S/N), charge resolution, amplitude, pre-pulse ratio (PPR), rise-time (RT), fall-time (FT), full width at half maximum (FWHM) and hit-time (HT) as in [12]. Please note all the potted PMTs were tested with a gain of around 1×10^7.

3.1 Noise level

The distribution of the waveform baseline is checked for all the 1F3 electronics channels. The sigma of a Gaussian fitting to the baseline distribution is used to evaluate the noise level of each electronic channel. The distribution of all the events of two individual electronic channels shows in figure 4(a) as an example. The noise level of each tested PMT with HV is shown in figure 4(b), and its mean value is around 0.4 mV. While the noise of some channels is larger, resulting in two smaller bumps in the distribution. The distance between the sub-peaks is around a minimum unit of the measurement.

The DCR can also be used to evaluate the electronic noise level by checking the relationship between the counting rate and threshold. A survey of DCR vs. threshold performs for all the electronic channels with and without HV and PMT. An example is shown in figure 4(c). We find that the DCR decreases when the threshold increases as expected, regardless of whether PMTs connected or not, after a plateau when the threshold is low.[2] The threshold location around 0.84 mV indicates the edge of the noise, which is around two times the baseline noise level in sigma. A threshold around 1.8 mV is suggested for PMT DCR measurements to avoid most of the noise which usually has a level of 0.3 mV–0.8 mV as shown in figure 4(b).



(a) Noise level (b) Noise level (c) DCR vs. threshold

Figure 4. Noise level of 1F3 electronics with or without PMTs connected. (a): the noise level of channel #21 and channel #24; (b): the noise level of all tested PMTs; (c): the threshold survey for DCR for one channel.

3.2 Waveform parameters

The digitization of PMT output waveforms provides more opportunities for a deeper understanding of the PMT features, and better precision is achieved with offline analysis. We will derive the waveform-related parameters with the recorded data in a single photoelectron (SPE) mode with the calibrated LED light source such as SPE amplitude, shape, and timing parameters.

[2]It is a source from the counting saturation when the noise is over the threshold all the time.

2023 JINST 18 P02003

A typical waveform with baseline deducted taken with container #D is shown in figure 5 with the traditional definition of the parameters, where the baseline is calculated from an interval of 75ns before each primary pulse, the rise-time (RT) is the time from 10% to 90% of the amplitude at the rising edge of the waveform, and the fall-time (FT) is the time from 90% to 10% of the amplitude at the falling edge. The FWHM is the time between 50% of the amplitude at the rising and falling edge, and the hit-time (HT) is the time over a threshold (3 mV) at the rising edge. The sigma σ of HT distribution is used as relative transit time spread (TTS[3]). An obvious overshoot in amplitude can be identified in the measured waveform. A few parameters are introduced to describe the features of overshoot: the primary pulse amplitude A_0, the peak time of the primary pulse T_0, the overshoot amplitude A_1, and the amplitude ratio A_1/A_0, the peak time of the overshoot T_1 and the recovery time of the overshoot T_2.[4]

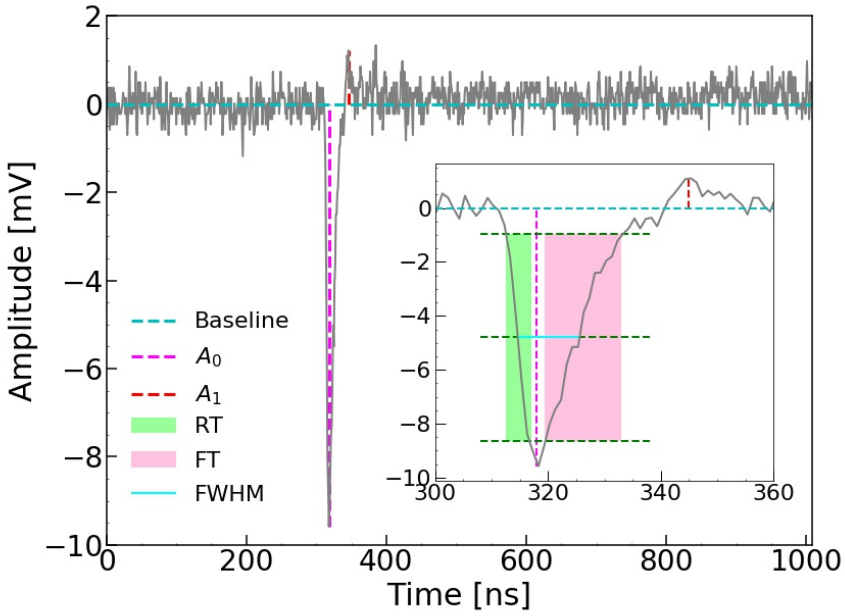


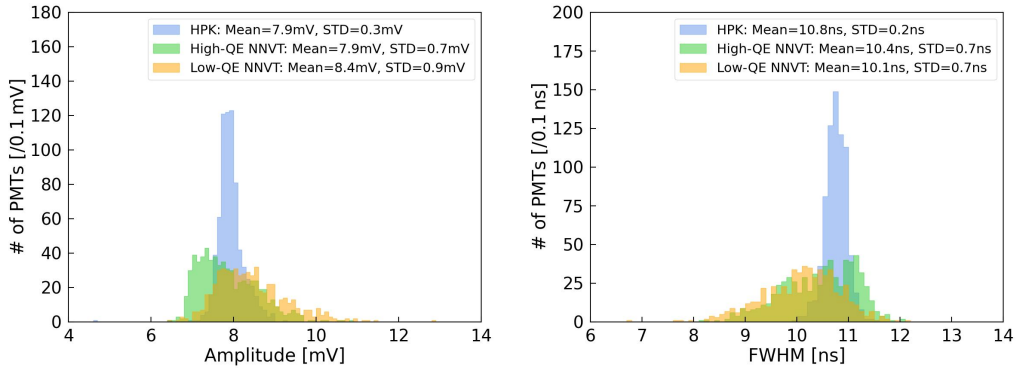
Figure 5. Exemplary of a typical NNVT waveform measured from container #D, and related parameters labeled.

In total, 738 dynode- and 1231 MCP- potted PMTs were tested with container #D, where the high-QE and low-QE MCP-PMTs are 655 and 576, respectively. Only the waveforms with amplitude larger than 3 mV are considered in the offline analysis to avoid possible noise. The average of each parameter is considered, some of which are shown in figure 6. The RT of MCP-PMTs is smaller than that of dynode PMTs, while the FT is opposite, so their FWHM is very similar. As shown in figure 6(a), the gain among the MCP-PMTs of NNVT shows a larger fluctuation, resulting in a broader distribution in amplitude.

[3]There is no laser system but only an LED light source installed in container #D, so the relative TTS is mainly contributed by the LED system and triggering.

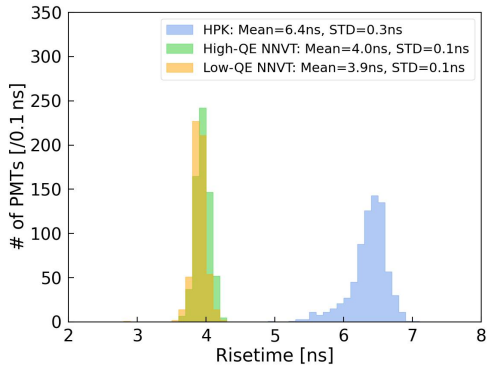
[4]T_2 is the time of the overshoot amplitude to recover to the baseline, which is calculated from an interval of 75ns before each primary pulse.

2023 JINST 18 P02003

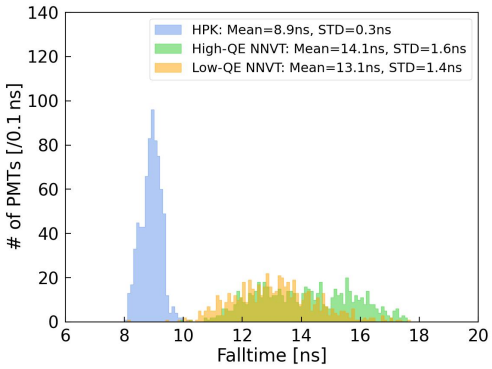


(a) SPE amplitude

(b) FWHM



(c) Rise-time



(d) Fall-time

Figure 6. Waveform parameters of SPE pulses of potted PMTs with 1F3 electronics. Top left: amplitude of SPE; top right: FWHM; bottom left: rise-time; bottom right: fall-time. Blue: HPK dynode PMTs; green: high-QE NNVT MCP-PMTs; orange: low-QE NNVT MCP-PMTs.

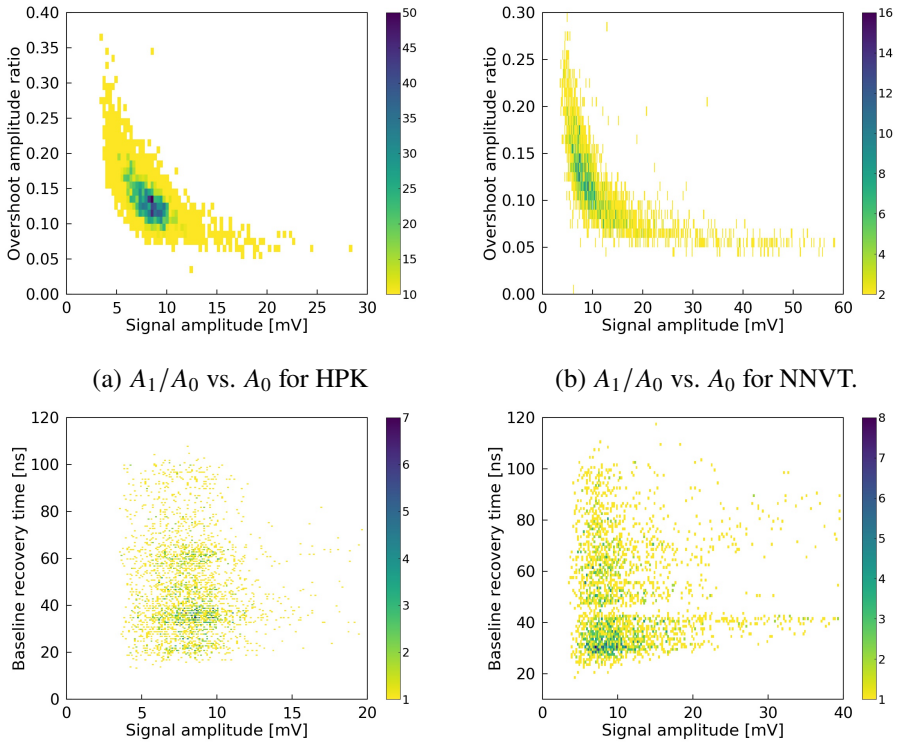
As known, the overshoot arises from the discharging of the split capacitor for the HV and PMT pulse of the HV divider with positive HV [24]. The typical overshoot parameters are summarised in table 1, where the pulse in the analysis is further selected with its waveform width larger than 5 ns, which results in a higher mean amplitude for the sample than for the SPE. The overshoot ratio to the primary pulse of SPE is around 13% for both types of PMTs, which is much larger than the previous testings with large signals in [24–26]. An example of the correlation between the overshoot ratio versus the amplitude of the primary pulse of a single PMT is shown in figure 7(a) and 7(b), where an anti-correlation can be found. It is because the overshoot is convoluted with the noise, which is dominant in the case of small signals such as SPE. After an FFT [27] filtering is applied to the waveforms, the overshoot ratio in amplitude decreases to around 9%, where the noise is suppressed partially. The overshoot peaked at around 44 ns after the peak of the primary pulse for both types of PMTs. The baseline of the overshoot recovers after around 49 ns for dynode PMTs and 51 ns for MCP-PMTs. An example of the correlation between the recovery time versus the amplitude of the primary pulse of a single PMT is shown in figure 7(c) and 7(d), and no obvious trend can be found.

The DCR of PMTs is related to the applied HV, PMT's temperature, and threshold. A threshold scan is done with one loading of container #D (32 potted PMTs in total), as shown in figure 8(a), where

2023 JINST 18 P02003

Table 1. Typical overshoot values of the potted PMTs with 1F3 electronics for the primary pulse in SPE.

Types	A_0/mV	A_1/mV	$T_1 - T_0/ns$	$T_2 - T_0/ns$	A_1/A_0
Dynode PMT	8.4	1.2	43.6	49.0	0.15
MCP-PMT	9.9	1.3	43.5	50.9	0.12



(a) A_1/A_0 vs. A_0 for HPK

(b) A_1/A_0 vs. A_0 for NNVT.

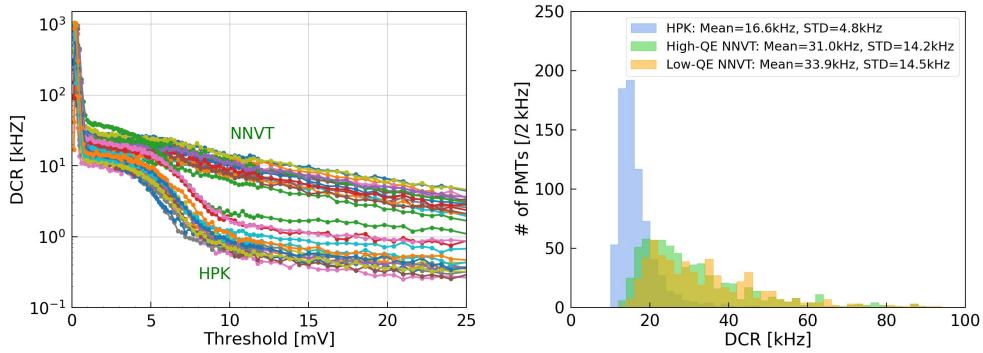
(c) $T_2 - T_0$ vs. A_0 for HPK.

(d) $T_2 - T_0$ vs. A_0 for NNVT.

Figure 7. Examples of a single PMT on the overshoot features versus the amplitude of the primary pulse. Top left: amplitude ratio of overshoot versus primary pulse amplitude for HPK; top right: amplitude ratio of overshoot versus primary pulse amplitude for NNVT; bottom left: baseline recovery time after overshoot versus primary pulse amplitude for HPK; bottom right: baseline recovery time after overshoot versus primary pulse amplitude for NNVT.

the NNVT MCP-PMTs show a higher DCR and a systematically longer tail than HPK dynode PMTs. Both types of PMTs show still a large counting rate when the threshold is higher than 25 mV, which is mainly due to events where a muon interacts with the PMT glass bulb [28]. For the system noise test, which is described in section 3.1 and the SPE amplitude, an amplitude threshold of around 1.8 mV is used for the PMT DCR measurement with container #D. Before the DCR measurement, a cooling time of at least 12 hours is used to stabilize the DCR after the PMT loading into the container and switching on the HV, which is in the following referred to as "cooling". During the DCR testing, the calibrated HV for a gain of around 1×10^7 is applied. The DCR distributions for both types of PMTs are shown in figure 8(b). The mean value is 16.6 kHz for HPK potted PMTs and 32.4 kHz for NNVT potted PMTs, respectively. Please note that the temperature of container #D is configured to 23°C.

2023 JINST 18 P02003



(a) Threshold vs. DCR

(b) Measured DCR

Figure 8. Threshold scan for DCR and the measured DCR of the tested PMTs. Left: threshold scan with one loading of container #D; right: measured DCR of all tested PMTs in container #D.

3.3 Charge parameters

There are a couple of studies on the charge de-convolution of PMT waveforms [29–32], for simplification we use the definition from the previous analysis, the charge (Q in pC) of each waveform here is integrated offline by summing all the samples in the target window with the baseline subtracted, where the loading impedance resistance (R) of 50 Ohm and the sampling rate are considered. According to the pulse shape, a target window of 75 ns is used: 20 ns in front of the pulse and 55 ns after the peak, and another 75 ns window is used to derive the baseline which is $[-95, -20]$ ns before the primary pulse peak. According to the above research on overshoot, the charge integral window includes the overshoot, and further study on the charge is in progress.

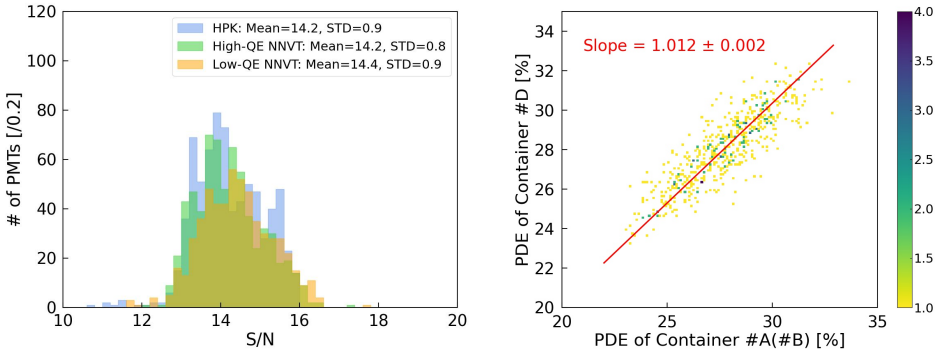
According to the testing procedure in [16], a working HV for a gain of around 1×10^7 is obtained through the HV-gain survey. The other parameters (P/V, S/N, charge resolution) were derived by SPE measurements with LED flashing following the previous definitions in [16] again. The reciprocal is taken in the calculation of the S/N. We can know that the average S/N is about 14 as shown in figure 9(a), which exceeds 10 and meets the noise requirement of 10% for containers.

The relative photon detection efficiency (PDE) is also determined in container #D after calibration, where the PDE measurement is performed with the LED in multi-photon mode to minimize systematic and statistical uncertainty [21]. Since the measured PDE is relative, only the PDE comparison of container #A(#B) and #D is shown in figure 9(b). From the fitting results, it is apparent that the two are consistent within 10% ranges. All typical parameter values with container #D and 1F3 electronics are collected in table 2. Another comparative analysis is discussed in section 4.

4 Comparison with commercial electronics

The noise level derived from the baseline distribution of containers #A and #B with PMTs connected is shown on the left of figure 10, the typical value is around 0.6 mV, which is slightly higher than container #D. The amplitude ratio of overshoot for containers #A and #B is also checked for both bare and potted PMTs as shown on the right of figure 10. It should be noted that these results are average values from SPE signals, so the amplitude ratio will be larger than the design due to the noise

2023 JINST 18 P02003



(a) S/N (b) PDE

Figure 9. The S/N and PDE distribution of potted PMTs in container #D. Green: HPK dynode PMTs; orange: nNVT MCP-PMTs.

Table 2. Typical parameters of dynode PMTs and MCP-PMTs in container #D. The corresponding uncertainties are shown in table 3.

Parameters	All PMT	Dynode PMT	MCP-PMT	High-QE PMT	Low-QE PMT
HV/V	1799	1929	1722	1701	1745
Gain/10^6	10.0	9.9	10.0	9.9	10.1
PDE/%	27.4	27.7	27.2	29.0	25.1
DCR /kHz	26.5	16.6	32.4	31.0	33.9
Resolution /%	30.5	28.0	32.0	32.7	31.2
P/V	3.8	3.6	3.9	3.9	3.9
FWHM/ns	10.5	10.8	10.3	10.4	10.1
S/N	14.3	14.2	14.3	14.2	14.4
RT/ns	4.8	6.4	3.9	4.0	3.9
FT/ns	11.9	8.9	13.6	14.1	13.1
HT/ns	314.0	285.4	331.1	331.8	330.2
Relative TTS /ns	8.8	6.2	10.3	10.3	10.4
Amplitude /mV	8.1	7.9	8.1	7.9	8.4

dominance. The mean value is 0.08 for bare PMTs with containers #A and #B and 0.06 for potted PMTs with containers #A and #B respectively, which is smaller than the results from container #D with 1F3 electronics prototype and potted PMTs, in particular, that of the potted PMTs. A larger overshoot will affect the charge measurement as discussed in [31] and the baseline recovery after a huge pulse. This is mainly due to the front-end cables, SHV connectors, and impedance matching inside the 1F3 electronics as shown in figure 11.

To monitor the system stability, five PMTs (three dynodes PMTs and two MCP-PMTs, as reference PMTs) are assigned to each of the containers #A and #B, and one dynode PMT and one MCP-PMT for container #D. One of the reference PMTs of each container is fixed in a drawer, and the others are surveyed for all the other channels. These PMTs participated in each

2023 JINST 18 P02003

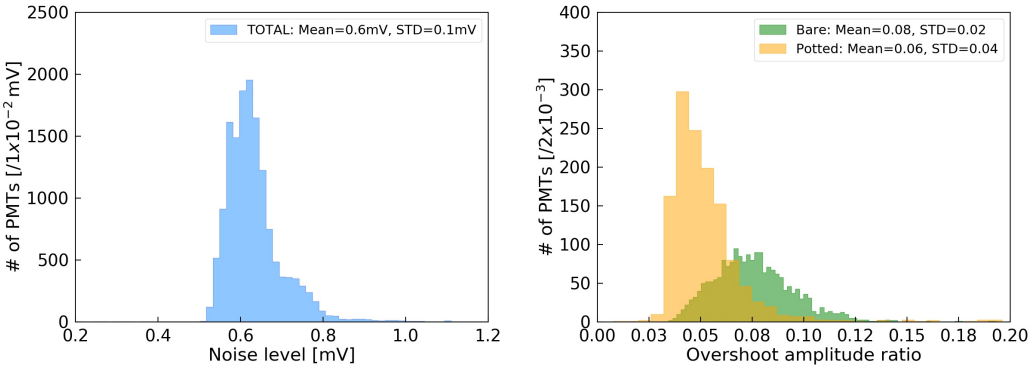


Figure 10. Left: noise level of baseline for containers #A and #B with PMTs connected; right: amplitude ratio of overshoot in containers #A and #B with bare/potted PMTs and commercial electronics.

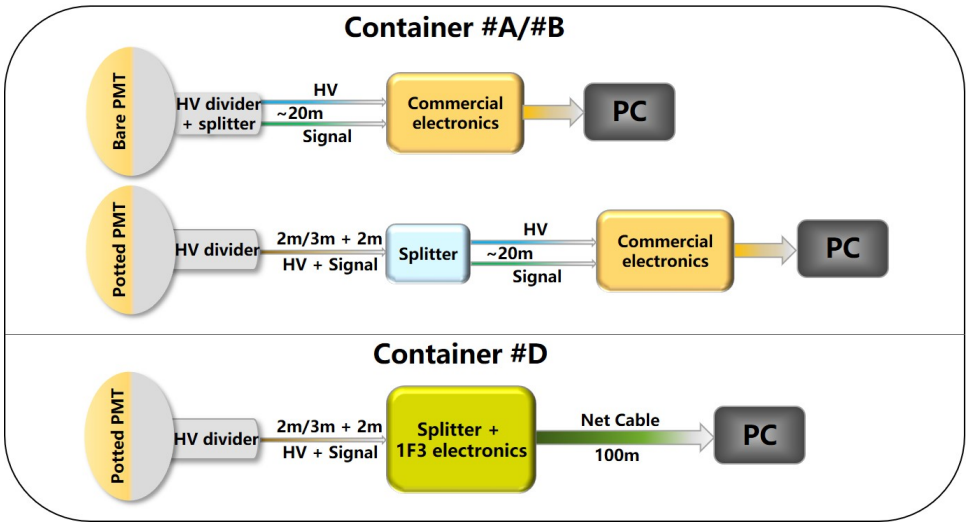


Figure 11. Comparison of cable and connections for the tests among containers #A, #B, and #D for bare and potted PMTs.

measurement throughout the testing task. The monitoring of the reference PMTs are used to check the reproducibility and stability of the containers, which also is taken as the measurement uncertainty. Each of the parameters for every container is fitted by a Gaussian function, and its σ is taken as the test error of the corresponding container. An average value is used for containers with more than one PMT of the same type. The reproducibility of all parameters of dynode PMTs and MCP-PMTs for each container is summarized in table 3.

To further quantify the difference, a parameter R is defined as eq. 4.1 to describe the relative inconsistency, where P_D and $P_{A(B)}$ are the values of PMTs tested in containers #D and #A (or #B) respectively, and $\bar{P} = \frac{1}{2}(P_D + P_{A(B)})$ is the mean. The R of each parameter is obtained by taking the mean value after filling the R of all PMTs into a histogram. And the error of R can be calculated by eq. 4.2, which combines the measurement error of containers and the error transfer formula. The R and its error of the two types of PMTs are summarized in table 4. Ignoring HT,[5] the R values of

[5]During the test, the power off and software sometimes reset, which may lead to the difference of several clocks

2023 JINST 18 P02003

Table 3. Uncertainties of dynode PMTs and MCP-PMTs for containers #A, #B, and #D.

Parameters	Dynode PMT			MCP-PMT		
	#A	#B	#D	#A	#B	#D
HV/V	7.0	6.7	6.8	7.1	9.7	15
Gain/10^6	0.14	0.16	0.11	0.29	0.31	0.32
PDE/%	0.72	0.79	0.47	1.1	0.88	0.52
DCR/kHz	3.3	2.0	1.4	7.4	5.4	3.3
Resolution/%	1.7	1.7	1.2	2.0	2.2	2.0
P/V	0.46	0.55	0.38	0.58	1.1	0.49
FWHM/ns	0.22	0.29	0.25	0.21	0.21	0.19
S/N	0.55	0.36	0.24	0.85	0.76	1.1
RT/ns	0.27	0.27	0.11	0.08	0.09	0.09
FT/ns	0.37	0.45	0.20	0.55	0.54	0.82
HT/ns	1.5	1.6	2.1	2.1	2.5	2.3
Relative TTS/ns	0.54	0.50	1.0	1.0	1.3	1.0
Amplitude/mV	0.15	0.14	0.17	0.34	0.43	0.23

all parameters are close to zero within the range of $[-\Delta_R, +\Delta_R]$, even most R values are accurate to the second and third decimal number. Therefore, we deduce that the parameter responses of the dynode PMTs and MCP-PMTs with the commercial electronics and 1F3 electronics prototype are consistent within the range of $[-\Delta_R, +\Delta_R]$.

$$R = \frac{P_D - \bar{P}}{\bar{P}} \tag{4.1}$$

$$\Delta_R = \frac{\sqrt{(P_{A(B)}\sigma_{P_D})^2 + (P_D\sigma_{P_{A(B)}})^2}}{2\bar{P}^2} \tag{4.2}$$

5 Summary

With this study, the basic features of the JUNO 1F3 electronics prototype used for 20-inch PMTs testing of container #D at JUNO Pan-Asia 20-inch PMT testing stations are checked, including noise level and PMT parameters. Among the PMT parameters calculated with the container #D 1F3 electronics, most of them except the overshoot ratio are consistent with previous acceptance tests with commercial electronics. The overshoot ratio in the case of the SPE signal is enlarged compared to the original design due to the extension cables, connectors, and impedance matching inside the electronics. Nevertheless, 1F3 electronics will still be used in the JUNO experiment, where there is no additional 2 m cable between PMT and 1F3 electronics, so the overshoot phenomenon should be improved to some extent. However, for a relatively large overshoot, it will affect the baseline recovery time after large signals, and affect the charge calculation caused by non-linearity. Therefore,

between HT of each channel, so the absolute value of HT is not significant and not compared directly.

2023 JINST 18 P02003

Table 4. The R and error of dynode PMT and MCP-PMT.

Parameters	Dynode PMT	MCP-PMT
HV	0.007 ± 0.003	0.002 ± 0.005
Gain	−0.002 ± 0.009	−0.009 ± 0.022
PDE	0.006 ± 0.016	0.008 ± 0.020
DCR	0.03 ± 0.11	−0.04 ± 0.13
Resolution	−0.005 ± 0.037	−0.007 ± 0.045
P/V	−0.03 ± 0.09	−0.02 ± 0.13
FWHM	0.05 ± 0.02	0.04 ± 0.01
S/N	0.05 ± 0.02	0.04 ± 0.05
RT	0.004 ± 0.023	0.05 ± 0.17
FT	−0.05 ± 0.02	−0.05 ± 0.04
HT	0.21 ± 0.005	0.190 ± 0.006
Relative TTS	−0.006 ± 0.091	0.02 ± 0.08
Amplitude	0.10 ± 0.02	0.07 ± 0.03

we will use the waveform analysis method to understand and evaluate the change and impact of overshoot in the JUNO experiment.

Acknowledgments

This work was supported by the National Natural Science Foundation (NSFC) of China No. 11875282, the Strategic Priority Research Program of the Chinese Academy of Sciences, Grant No. XDA10011100, the CAS Center for Excellence in Particle Physics, the Joint Institute of Nuclear Research (JINR), Russia and Lomonosov Moscow State University in Russia, the joint Russian Science Foundation (RSF), DFG (Deutsche Forschungsgemeinschaft). The authors acknowledge all colleagues from JUNO collaboration for operating the 20-inch PMT testing system.

References

[1] Daya Bay collaboration, *Measurement of electron antineutrino oscillation based on 1230 days of operation of the Daya Bay experiment*, *Phys. Rev. D* **95** (2017) 072006 [arXiv:1610.04802].

[2] RENO collaboration, *Observation of Reactor Electron Antineutrino Disappearance in the RENO Experiment*, *Phys. Rev. Lett.* **108** (2012) 191802 [arXiv:1204.0626].

[3] Double Chooz collaboration, *Reactor electron antineutrino disappearance in the Double Chooz experiment*, *Phys. Rev. D* **86** (2012) 052008 [arXiv:1207.6632].

[4] JUNO collaboration, *JUNO Conceptual Design Report*, arXiv:1508.07166.

[5] JUNO collaboration, *Neutrino Physics with JUNO*, *J. Phys. G* **43** (2016) 030401 [arXiv:1507.05613].

[6] L.-J. Wen, M. He, Y.-F. Wang, J. Cao, S.-L. Liu, Y.-K. Heng et al., *A quantitative approach to select PMTs for large detectors*, *Nucl. Instrum. Meth. A* **947** (2019) 162766 [arXiv:1903.12595].

2023 JINST 18 P02003

[7] Northern Night Vision Technology Ltd, *Specification for GDB-6201 microchannel plate type photomultiplier PMT*, 2019 [in Chinese].

[8] Hamamtsu Photonics K.K., *R12860 datasheet*, 2019, https://www.hamamatsu.com/jp/en/product/type/R12860/index.html.

[9] JUNO collaboration, *JUNO physics and detector*, *Prog. Part. Nucl. Phys.* **123** (2022) 103927 [arXiv:2104.02565].

[10] Y. Wang et al., *A new design of large area MCP-PMT for the next generation neutrino experiment*, *Nucl. Instrum. Meth. A* **695** (2012) 113.

[11] L. Ren et al., *Study on the improvement of the 20-inch microchannel plate photomultiplier tubes for neutrino detector*, *Nucl. Instrum. Meth. A* **977** (2020) 164333.

[12] JUNO collaboration, *Mass testing and characterization of 20-inch PMTs for JUNO*, *Eur. Phys. J. C* **82** (2022) 1168 [arXiv:2205.08629].

[13] JUNO collaboration, *Signal Optimization with HV divider of MCP-PMT for JUNO*, *Springer Proc. Phys.* **213** (2018) 309 [arXiv:1803.03746].

[14] Z. Qin, *Status of the 20-in. PMT Instrumentation for the JUNO Experiment*, *Springer Proc. Phys.* **213** (2018) 285.

[15] JUNO collaboration, *JUNO physics and detector*, *Prog. Part. Nucl. Phys.* **123** (2022) 103927 [arXiv:2104.02565].

[16] B. Wonsak et al., *A container-based facility for testing 20'000 20-inch PMTs for JUNO*, 2021 *JINST* **16** T08001 [arXiv:2103.10193].

[17] JUNO collaboration, *Large photocathode 20-inch PMT testing methods for the JUNO experiment*, 2017 *JINST* **12** C06017 [arXiv:1705.05012].

[18] CAEN S.p.A., *User Manual UM4279 - V1742/VX1742: 32+2 Channel 12bit 5 GS/s Switched Capacitor Digitizer*, rev. 7, CAEN S.p.A., Viareggio, Italy (2017).

[19] JUNO collaboration, *The JUNO experiment and its electronics readout system*, 2022 *JINST* **17** C05014 [arXiv:2110.12277].

[20] HVSys Company, *Light emitting diode sources of calibrated short light flashes*, http://hvsys.ru/images/data/news/10_small_1368803142.pdf, 2013.

[21] N. Anfimov, A. Rybnikov and A. Sotnikov, *Optimization of the light intensity for Photodetector calibration*, *Nucl. Instrum. Meth. A* **939** (2019) 61 [arXiv:1802.05437].

[22] M. Bellato et al., *Embedded readout electronics R&D; for the large PMTs in the JUNO experiment*, *Nucl. Instrum. Meth. A* **985** (2021) 164600 [arXiv:2003.08339].

[23] T. Zhou, X. Ji, K. Zhu and F. Li, *DAQ readout prototype for JUNO*, *Rad. Det. Tech. Meth.* **5** (2021) 600.

[24] JUNO collaboration, *Signal Optimization with HV divider of MCP-PMT for JUNO*, *Springer Proc. Phys.* **213** (2018) 309 [arXiv:1803.03746].

[25] F.-J. Luo et al., *PMT overshoot study for the JUNO prototype detector*, *Chin. Phys. C* **40** (2016) 096002 [arXiv:1602.06080].

[26] H.Q. Zhang et al., *Comparison on PMT Waveform Reconstructions with JUNO Prototype*, 2019 *JINST* **14** T08002 [arXiv:1905.03648].

[27] CERN ROOT, *Fast Fourier Transforms tutorials*, https://root.cern/doc/master/group__tutorial__fft.html 2020.

2023 JINST 18 P02003

[28] Y. Zhang, Z. Wang, M. Li, Y. Zhang, Y. Wang, Z. Peng et al., *Study of 20-inch PMTs dark count generated large pulses*, 2022 *JINST* **17** P10048 [arXiv:2206.07456].

[29] S. Jetter, D. Dwyer, W.-Q. Jiang, D.-W. Liu, Y.-F. Wang, Z.-M. Wang et al., *PMT waveform modeling at the Daya Bay experiment*, *Chin. Phys. C* **36** (2012) 733.

[30] Y. Huang et al., *The Flash ADC system and PMT waveform reconstruction for the Daya Bay Experiment*, *Nucl. Instrum. Meth. A* **895** (2018) 48 [arXiv:1707.03699].

[31] H.Q. Zhang et al., *Comparison on PMT Waveform Reconstructions with JUNO Prototype*, 2019 *JINST* **14** T08002 [arXiv:1905.03648].

[32] D. Xu et al., *Towards the ultimate PMT waveform analysis for neutrino and dark matter experiments*, 2022 *JINST* **17** P06040 [arXiv:2112.06913].

2023 JINST 18 P02003